

Helical edge magnetoplasmon in the quantum Hall effect regime

Sanderson Silva¹ and O. G. Balev^{1, a)}

Departamento de Física, Universidade Federal do Amazonas, 69077-000, Manaus, Amazonas, Brazil

(Dated: 27 May 2018)

We present the microscopic treatment of edge magnetoplasmons (EMPs) for the regime of not-too-low temperatures defined by the condition $\hbar\omega_c \gg k_B T \gg \hbar v_g/2\ell_0$, where v_g is the group velocity of the edge states, $\ell_0 = \sqrt{\hbar/m^*\omega_c}$ is the magnetic length and ω_c is the cyclotron frequency. We find a weakly damped symmetric mode, named helical edge magnetoplasmon, which is localized at the edge states region for filling factors $\nu = 1, 2$ and *very strong dissipation* $\eta_T = \xi/k_x \ell_T \gtrsim \ln(1/k_x \ell_T) \gg 1$, where the characteristic length $\ell_T = k_B T \ell_0^2/\hbar v_g \gg \ell_0/2$ with ξ being the ratio of the local transverse conductivity to the local Hall conductivity at the edge states and k_x is the wave vector along the edge; here other EMP modes are strongly damped. The spatial structure of the helical edge magnetoplasmon, transverse to the edge, is strongly modified as the wave propagates along the edge. In the regime of *weak dissipation*, $\eta_T \ll 1$, we obtain exactly the damping of the fundamental mode as a function of k_x . For $\nu = 4$ and weak dissipation we find that the fundamental modes of $n = 0$ and $n = 1$ Landau levels (LLs) are strongly renormalized due to the Coulomb coupling. Renormalization of all these EMPs coming from a metal gate and air half-space is studied.

PACS numbers: 73.43.Lp, 73.43.-f

Keywords: Edge Magnetoplasmons, Quantum Hall Effect

I. INTRODUCTION

Edge magnetoplasmons (EMPs) in the two-dimensional electron system (2DES) are chiral collective excitations propagating along the edge of the 2DES in the presence of a normal magnetic field B . They have received much attention after pioneering works in the 80's.¹⁻³ Many experimental studies have been performed for confined electrons in AlGaAs-GaAs heterostructures^{1,4-18} and for surface electrons on liquid helium.^{2,3,19} The advent of time-resolved techniques^{8,10,12,15} and recent experimental techniques based on B -periodic oscillations in the photovoltage and in the longitudinal resistance of 2DES, induced by microwave radiation and attributed to the interference of coherently excited EMPs,¹⁶⁻¹⁸ increases greatly the interest in EMPs studies. EMPs are sensitive to reconstruction of quantum Hall edges^{20,21} and can probe the interactions properties in a quantum Hall line junction system.²² A lot of theoretical works have investigated the characteristics of EMPs and different edge-wave mechanisms are proposed or used.²⁰⁻³⁷

Theoretically EMPs often are studied employing models entirely classical, see *e.g.* Refs.^{24,26}. In these edge-wave mechanisms the charge density varies at the 2DES edge, but the position of the 2DES edge is kept constant. Different, quantum-mechanical edge-wave mechanisms are developed in Refs.^{20,25,27,28}. In these models only the edge of 2DES is varying while the density profile, with respect to the fluctuating edge, coincides with that of the unperturbed 2DES. Recently, a microscopic model

has been proposed in Refs.^{31,32} that effectively incorporates both above edge-wave mechanisms in the quantum Hall effect (QHE) regime.

The study of the EMPs with this new edge-wave mechanism is elaborated in Refs.³¹⁻³³ in the limit of low temperatures given by $k_B T \ll \hbar v_g/2\ell_0$, where v_g is the group velocity of the edge states and the magnetic length $\ell_0 = \sqrt{\hbar/m^*\omega_c}$ with the cyclotron frequency $\omega_c = |e|B/m^*c$. Later, the approach of Refs.^{31,32} has been extended in Ref.³⁴ for not-too-low temperatures such that $\hbar\omega_c \gg k_B T \gg \hbar v_g/2\ell_0$, where the typical scale of in-plane components of the wave electric field \mathbf{E} is of the order of the characteristic length $\ell_T = \ell_0^2 k_B T/\hbar v_g \gg \ell_0/2$. In Ref.³⁴ it is shown that the main contribution to the damping of EMPs is given by dissipation effects localized within a narrow region of width of the order of ℓ_T , nearby the edge states. For $\nu = 1, 2$, weakly damped EMPs are obtained in Ref.³⁴ only in the *weak dissipation* regime $\eta_T \ll 1$ or in the *strong dissipation* regime defined by $\ln(1/k_x \ell_T) \gg \eta_T \gtrsim 1$ and for homogeneous samples (*i.e.*, without gate or air region close to the 2DES).

In the present paper the microscopic approach of Ref.³⁴ is extended to study EMPs at *not-too-low temperatures* both in homogeneous samples and in samples with a metal gate or air on the top of the sample at distance d from the 2DES. We study, at $\nu = 1, 2$, EMPs for very strong dissipation at the edge, *i.e.*, for $\eta_T \gtrsim \ln(1/k_x \ell_T) \gg 1$, and a new weakly damped mode, which we call *helical edge magnetoplasmon* or *edge helicon*, is obtained. In particular, we obtain that the real part of helical edge magnetoplasmon frequency $Re\omega$ for the homogeneous sample and very strong dissipation almost coincides with that of the fundamental EMP, obtained in Ref.³⁴ for $\eta_T \ll 1$. This result is rather unexpected because, in particular, all other EMPs (calculated

^{a)}Electronic mail: ogbalev@ufam.edu.br

from the same secular determinant as the helical edge magnetoplasmon mode) are now strongly damped, with $Re\omega/(-Im\omega) \sim 1/\eta_T \ll 1$. We show that the spatial structure of the helical edge magnetoplasmon, transverse to the edge, is strongly modified as the wave propagates along the edge. In addition, for the gated sample and *weak dissipation*, $\eta_T \ll 1$, the acoustic-like dispersion for the fundamental mode is found for some ranges of k_x and comparison with pertinent qualitative estimations of Ref.³⁸ is given. Finally, we study the fundamental modes of $n = 0$ and $n = 1$ LLs and their strong renormalization due to the Coulomb coupling for $\nu = 4$. and weak dissipation, $\eta_T \ll 1$,

We emphasize three essential points that we take into account in our approach in order to determine the dispersion relation as well the spatial structures of the EMPs. The first one is the role of dissipation that is mainly localized at the edge states when a smooth lateral confinement is assumed and $\hbar\omega_c/k_B T \gg 1$ ³⁹; it is related with the scattering by acoustic phonons and becomes exponentially small for $v_g < s$ in comparison with the case $v_g > s$, where s is the speed of sound. The second one is the very realistic form of the unperturbed electron density $n_0(y)$ across the edge. It was shown³⁴ that for not-too-low temperatures and $\nu = 1, 2$ the density profile $n_0(y)$ is well approximated by $n_0(y)/n_0 = [1 - \tanh(Y/2)]/2$, where $Y = (y - y_{re})/\ell_T$ with y_{re} being the edge of the $n = 0$ LL when the condition $k_e \gg k_B T/\hbar v_g \gg 1/2\ell_0$ is fulfilled. Here the characteristics edge wave number $k_e = (\omega_c/\hbar\Omega)\sqrt{2m^*\Delta_F}$, where Δ_F is the Fermi energy measured from the bottom of the $n = 0$ LL, i.e., $\Delta_F = E_{F0} - \hbar\omega_c/2$; n_0 is the density in the interior part of the channel and E_{F0} is the Fermi level measured from the bottom of the lowest electric subband. In addition, we show here that the density profile is more complicated for $\nu = 4$ (see the solid curve in Fig. 8): the steep drop of $n_0(y)$ at the edge is splitted in two steps - one is centered at the $n = 0$ LL edge, y_{re} , and the other step is centered at the $n = 1$ LL edge, $y_{re}^{(1)}$.

The third point is related with effects of the strong electron-electron interaction in the EMPs. In particular, at $\nu = 1, 2$, the weakly damped helical edge magnetoplasmon mode is manifested, for the regime of very strong dissipation, only due to the strong self-consistent electron-electron interaction. Indeed, if we assume that the electron-electron interaction is weak then this mode becomes strongly damped as any other EMP mode. In particular, by neglecting the coupling of the monopole term (the main term for the helical edge magnetoplasmon) with any multipole term we obtain for the homogeneous sample and $k_x\ell_T \ll 1$, according to Ref.³⁴, that $Re\omega/(-Im\omega) \approx [4\ln(1/k_x\ell_T)]/(3\eta_T) \ll 1$ for typical conditions of our Fig. 2. I.e., in this crude approximation the mode is strongly damped. However, the exact results for the helical edge magnetoplasmon presented in Fig. 2 shows that $Re\omega/(-Im\omega) > 17$. Point out, very close gate also can essentially suppress electron-electron interaction within 2DES. Further, for $\nu = 4$, electron-

electron interaction leads to strong Coulomb coupling of the fundamental EMP of $n = 0$ LL with the fundamental EMP of $n = 1$ LL, resulting in strong renormalization of their dispersion relations.

We show here that the combination of these factors strongly modifies properties of the EMPs. In addition, it deserves to be pointed out that a many-body study of LLs spectra, at $\nu = 1$, nearby the edge states show⁴⁰ that electron correlations can essentially facilitate the appearance of not-too-low temperatures regime (in particular, for $T \sim 1$ K): as the renormalized group velocity v_g can become⁴⁰ $\propto T$ for $4.2\text{K} \gtrsim T \gtrsim 0.3\text{K}$.

The organization of the paper is as follows. In Sec. II we present briefly the general formalism³⁴ for $\nu = 1, 2$ with the modifications that appear due to the gate or the air half-space. In Sec. III A we study the integral equations for symmetric and antisymmetric EMPs for $\eta_T \gg 1$ and obtain the frequency spectrum and the spatial behavior of the helical edge magnetoplasmon. We consider also the effect of the gate and the air half-space. In Sec. III B we treat symmetric and antisymmetric EMPs in the weak dissipation regime, $\eta_T \ll 1$. In Sec. IV, we study the fundamental EMPs of $n = 0$ LL and $n = 1$ LL and their coupling by Coulomb interaction for $\nu = 4$ and in the weak dissipation regime. Finally, in Sec. V, we make the concluding remarks.

II. INTEGRAL EQUATIONS FOR EMPs AT $\nu = 1, 2$

Our model consists of a 2DES with width W , length $L_x = L$, and zero thickness, in the presence of a strong B parallel to the z axis. The lateral confining potential V'_y of the 2DES, semi-parabolic at the left and right edges of the channel, is given as

$$\begin{aligned} V'_y &= 0, \text{ for } y_l < y < y_r, \\ V'_y &= \frac{m^*\Omega^2}{2}(y - y_r)^2, \text{ for } y > y_r > 0, \\ \text{and } V'_y &= \frac{m^*\Omega^2}{2}(y - y_l)^2, \text{ for } y < y_l < 0. \end{aligned} \quad (1)$$

We assume that the confinement is smooth on the scale of ℓ_0 (i.e., $\Omega \ll \omega_c$) and $|k_x|W \gg 1$. Then it is possible to consider an EMP⁴¹ $A(\omega, k_x, y) \exp[-i(\omega t - k_x x)]$ only along, e.g., the right edge of the channel. For $\nu = 1$, we assume that the spin-splitting, caused by many-body effects, is strong enough to neglect the contribution from the upper spin-split LL. For $\nu = 2$ and 4, we neglect spin-splitting. To simplify notations, we omit superscript or subscript 0 in values pertinent to $n = 0$ LL like $v_{g0} \equiv v_g$, $\Delta_{F0} \equiv \Delta_F$, $k_e^{(0)} \equiv k_e$, etc. For definiteness, the 2DES is considered in GaAs based sample.

At the $\nu = 1, 2$ QHE regime, with $\hbar\omega_c \gg k_B T \gg \hbar v_g/\ell_0$, for $\omega \ll \omega_c$ the current density components induced by an EMP have both quasistatic and local (due to $\min\{1/k_x, \ell_T\} \gg \ell_0$) form³⁴

$$\begin{aligned} j_x(y) &= \sigma_{yy}(y)E_x(y) - \sigma_{yx}^0(y)E_y(y) + v_g\rho(\omega, k_x, y), \\ j_y(y) &= \sigma_{yy}(y)E_y(y) + \sigma_{yx}^0(y)E_x(y), \end{aligned} \quad (2)$$

where in the wave current density, $j_\mu(y)$, and the wave electric field, $E_\mu(y)$, the wave factor $\exp[-i(\omega t - k_x x)]$, and the arguments ω , k_x are suppressed; $\rho(\omega, k_x, y)$ is the wave electron charge density and $\sigma_{\mu\nu}$ are the components of the conductivity tensor. Here, cf. with Refs.^{34,39}, $\sigma_{yy}(y) = \sigma_{xx}(y) \approx \tilde{\sigma}_{yy}R_0(\bar{y})$, with $R_0(\bar{y}) = (4\ell_T)^{-1} \cosh^{-2}(\bar{y}/2\ell_T)$ and $\bar{y} = y - y_{re}$, is defined by nonelastic scattering within the edge states region on acoustic phonons. Notice, additional study justifies approximation of the diagonal conductivity only by its dissipative (or real) part; so $\sigma_{yy}(y)$ is strongly localized within a distance $\lesssim \ell_T$ from the edge states (the intersection of LL with the Fermi level). For GaAs based sample the main contribution to $\tilde{\sigma}_{yy}$ is due to piezoelectric acoustic(PA)-phonons; in particular, for $v_g \geq s$ and $\nu = 1$ we have that $\tilde{\sigma}_{yy} = e^2 \ell_0^2 c' k_B T / 4\pi^2 \hbar^4 v_g^3$, where the electron-phonon coupling constant $c' = \hbar(eh_{14})^2 / 2\rho_V s$, with $h_{14} = 1.2 \times 10^7 \text{V/cm}$, $\rho_V = 5.31 \text{g/cm}^3$, and $s = 2.5 \times 10^5 \text{cm/sec}$; $\epsilon = 12.5$. Hereafter we are using these parameters in numerical estimates and results shown in the figures.

For $\nu = 1, 2$ we have

$$\sigma_{yx}^0(y) \approx \sigma_{yx}^0 [1 + e^{(E_0(y) - E_{F0})/k_B T}]^{-1}, \quad (3)$$

where $E_n(y) = \hbar\omega_c(n + 1/2) + V_y'$, $\sigma_{yx}^0 = e^2\nu/2\pi\hbar$ is the value of the local Hall conductivity $\sigma_{yx}^0(y)$ in the interior part of the channel; $\sigma_{yx}^0(y_{re}) = \sigma_{yx}^0/2$. For $k_e \gg k_B T/\hbar v_g \gg 1/2\ell_0$ we obtain³⁴ that $d\sigma_{yx}^0(y)/dy \approx -(e^2\nu/2\pi\hbar)R_0(\bar{y})$; the group velocity $v_g = (\ell_0^2/\hbar)dE_0(y_{re})/dy = \hbar\Omega^2 k_e/m^* \omega_c^2$. Then using Eqs. (2), (3), the Poisson equation, and the linearized continuity equation we obtain the integral equation for the wave electron charge density as

$$\begin{aligned} -i(\omega - k_x v_g)\rho(\omega, k_x, y) + \frac{2}{\epsilon}\{k_x^2 \sigma_{yy}(y) - ik_x \frac{d}{dy}[\sigma_{yx}^0(y)] \\ - \sigma_{yy}(y) \frac{d^2}{dy^2} - \frac{d}{dy}[\sigma_{yy}(y)] \frac{d}{dy}\} \int_{-\infty}^{\infty} dy' [K_0(|k_x||y - y'|) \\ + \beta K_0(|k_x|\sqrt{(y - y')^2 + 4d^2})] \rho(\omega, k_x, y') = 0, \end{aligned} \quad (4)$$

where $K_0(x)$ is the modified Bessel function. For $\beta = 0$, Eq. (4) corresponds to a sample with the homogeneous background dielectric constant ϵ , whereas for $\beta = -1$ or $\beta = (\epsilon - 1)/(\epsilon + 1)$ it corresponds to a sample with the metallic gate or air half-plane at a distance d from the 2DES.

Any solution $\rho(\omega, k_x, y) \equiv \rho(\omega, k_x, \bar{y})$ of Eq. (4) is either symmetric or antisymmetric with respect to the change $\bar{y} \rightarrow -\bar{y}$; i.e., with respect to the right edge, y_{re} . Then straightforwardly it follows from Eq. (4) two integral equations. One for symmetric EMP modes, with

$\rho^s(\omega, k_x, \bar{y}) = \rho^s(\omega, k_x, -\bar{y})$, and other for antisymmetric EMP modes, with $\rho^a(\omega, k_x, \bar{y}) = -\rho^a(\omega, k_x, -\bar{y})$, as

$$\begin{aligned} (\omega - k_x v_g)\rho^{s,a}(\omega, k_x, \bar{y}) - \frac{2}{\epsilon}\{(k_x \sigma_{yx}^0 - ik_x^2 \tilde{\sigma}_{yy})R_0(\bar{y}) \\ + i\tilde{\sigma}_{yy} \frac{d}{d\bar{y}}[R_0(\bar{y}) \frac{d}{d\bar{y}}]\} \int_0^\infty d\bar{y}' \{[K_0(|k_x||\bar{y} - \bar{y}'|) \\ + \beta K_0(|k_x|\sqrt{(\bar{y} - \bar{y}')^2 + 4d^2})] \pm [K_0(|k_x||\bar{y} + \bar{y}'|) \\ + \beta K_0(|k_x|\sqrt{(\bar{y} + \bar{y}')^2 + 4d^2})]\} \rho^{s,a}(\omega, k_x, \bar{y}') = 0, \end{aligned} \quad (5)$$

where and hereafter the upper (lower) sign corresponds to symmetric (antisymmetric) EMPs.

Solutions of Eq.(5), for $\bar{y} \geq 0$, are given as

$$\rho^{s,a}(\omega, k_x, \bar{y}) = \tilde{R}_0(Y) e^{-Y} \sum_{n=0}^{\infty} \rho_n^{s,a}(\omega, k_x) L_n(Y), \quad (6)$$

where $Y = \bar{y}/\ell_T$, $L_n(Y)$ is the Laguerre polynomial, $\tilde{R}_0(Y) = (4\ell_T)^{-1} \exp(Y) \cosh^{-2}(Y/2)$. For $\bar{y} \leq 0$, the expression for $\rho^s(\omega, k_x, \bar{y})$ follows from Eq. (6) by using $|Y|$ in the RHS of Eq.(6). As $\rho^a(\omega, k_x, 0) = 0$ for antisymmetric EMPs it follows from Eq.(6) that

$$\sum_{n=0}^{\infty} \rho_n^a(\omega, k_x) = 0. \quad (7)$$

For $\bar{y} < 0$, $\rho^a(\omega, k_x, \bar{y})$ is defined by Eq.(6) and the odd-parity property.

Finally, the symmetric and antisymmetric modes are defined by

$$\begin{aligned} (\omega - k_x v_g)\rho_m^{s,a}(\omega, k_x) - \sum_{n=0}^{\infty} [S r_{mn}^{s,a}(k_x) \\ + S' g_{mn}^{s,a}(k_x)] \rho_n^{s,a}(\omega, k_x) = 0, \end{aligned} \quad (8)$$

where $S = (2/\epsilon)(k_x \sigma_{yx}^0 - ik_x^2 \tilde{\sigma}_{yy})$, $S' = -2i\tilde{\sigma}_{yy}/\epsilon\ell_T^2$,

$$\begin{aligned} r_{mn}^{s,a}(k_x) &= \ell_T \int_0^\infty dx e^{-x} L_m(x) \\ &\times \int_0^\infty dx' \{[K_0(|k_x|\ell_T|x - x'|) \\ + \beta K_0(|k_x|\ell_T\sqrt{(x - x')^2 + (2d/\ell_T)^2})] \\ &\pm [K_0(|k_x|\ell_T|x + x'|) \\ + \beta K_0(|k_x|\ell_T\sqrt{(x + x')^2 + (2d/\ell_T)^2})]\} \\ &\times \tilde{R}_0(x') e^{-x'} L_n(x'), \end{aligned} \quad (9)$$

and

$$\begin{aligned}
g_{mn}^{s,a}(k_x) &= |k_x| \ell_T^2 \int_0^\infty dx e^{-x} \{ e^{-x/2} L_m(x) / \cosh(x/2) \\
&- \frac{m}{x} [L_m(x) - L_{m-1}(x)] \} \\
&\times \int_0^\infty dx' \{ [\text{sign}\{x-x'\} K_1(|k_x| \ell_T |x-x'|) \\
&+ \beta \frac{(x-x') K_1(|k_x| \ell_T \sqrt{(x-x')^2 + (2d/\ell_T)^2})}{\sqrt{(x-x')^2 + (2d/\ell_T)^2}}] \\
&\pm [K_1(|k_x| \ell_T (x+x')) \\
&+ \beta \frac{(x+x') K_1(|k_x| \ell_T \sqrt{(x+x')^2 + (2d/\ell_T)^2})}{\sqrt{(x+x')^2 + (2d/\ell_T)^2}}] \} \\
&\times \tilde{R}_0(x') e^{-x'} L_n(x') + \delta g_{mn}^{s,a}(k_x). \tag{10}
\end{aligned}$$

Here $\text{sign}\{x\} = 1$ for $x > 0$ and $\text{sign}\{x\} = -1$ for $x < 0$, $K_1(x)$ is the modified Bessel functions. In addition, $\delta g_{mn}^s(k_x) \equiv 0$ and

$$\begin{aligned}
\delta g_{mn}^a(k_x) &= 2|k_x| \ell_T^2 \int_0^\infty dx [K_1(|k_x| \ell_T x) \\
&+ \beta \frac{x K_1(|k_x| \ell_T \sqrt{x^2 + (2d/\ell_T)^2})}{\sqrt{x^2 + (2d/\ell_T)^2}}] \tilde{R}_0(x) e^{-x} L_n(x). \tag{11}
\end{aligned}$$

Point out, for antisymmetric EMPs, due to Eq.(7) the logarithmically divergent contributions from the terms Eq.(11) are mutually cancelled, after the summation over n in Eq.(8). Hereafter we drop k_x in $r_{mn}^{s,a}(k_x)$ and $g_{mn}^{s,a}(k_x)$ to simplify the notation; notice that $r_{mn}^{s(a)} \neq r_{nm}^{s(a)}$, $g_{mn}^{s(a)} \neq g_{nm}^{s(a)}$.

In the solution of Eqs. (8)-(11), we are taking the long-wavelength limit $|k_x| \ell_T \ll 1$. As a result, for $\beta = 0$ we can use the approximation $K_0(|k_x| \ell_T x) \approx \ln(2/|k_x| \ell_T) - \gamma - \ln(x)$ and $K_1(|k_x| \ell_T x) \approx (|k_x| \ell_T x)^{-1}$, where γ is the Euler constant. However, for $\beta \neq 0$ when $(2d/\ell_T)^2 \gg 1$, such that $2|k_x|d \gtrsim 1$, we will use exact expressions for pertinent modified Bessel functions. We also will denote $\bar{\omega} = \omega - k_x v_g$, where typically $v_g \ll \omega/k_x$ for the most fast EMP modes, i.e., the renormalized monopole EMPs. So the main contribution to their phase velocity, ω/k_x , is given by $\bar{\omega}/k_x$. The latter contribution is due to the electron-electron interactions induced by wave excitation.

For definiteness, if otherwise it is not stated, we consider 2DES in the homogeneous sample, i.e., without the gate or the air half-plane.

III. EMPS AT $\nu = 1, 2$

Point out, we can neglect the intermode coupling by omitting in Eq.(8) all nondiagonal coefficients $r_{m,n}^{s,a}$ and $g_{m,n}^{s,a}$, i.e., with $m \neq n$. Then from Eqs.(6), (8) it follow pure symmetric modes (monopole, only $\rho_0^s \neq 0$, quadrupole, only $\rho_1^s \neq 0$, etc.) or pure antisymmetric modes (dipole, only $\rho_{0,1}^a \neq 0$, etc.). However, coupling

among the ‘‘neighboring’’ pure modes⁴² due to nondiagonal, $m \neq n$, coefficients $r_{m,n}^{s,a}$ and $g_{m,n}^{s,a}$ typically is strong and especially for *very strong dissipation*. So the coupling between different pure modes should be taken into account. This leads to renormalized modes, which there are true EMPs. In particular, the modification of dissipation strength from *the weak dissipation* to *very strong dissipation* should strongly effect the characteristics of renormalized EMPs. The latter ones we call also as EMPs. For the assumed long-wavelength limit $k_x \ell_T \ll 1$ we define the weak, strong and very strong dissipative regimes more precisely by the conditions $\eta_T \ll 1$, $\ln(1/k_x \ell_T) \gg \eta_T \gtrsim 1$ and $\eta_T \gtrsim \ln(1/k_x \ell_T) \gg 1$, respectively; $\eta_T = \xi/k_x \ell_T$ where $\xi = \tilde{\sigma}_{yy}/(\ell_T \sigma_{yx}^0)$, notice, $|S'|/S = \eta_T$. Because the magnetic field is strong it follows that $\xi \ll 1$. However, as $k_x \ell_T \ll 1$ the regime of very strong dissipation can be easily achieved if $v_g \geq s$.

Point out, similar regimes (conditions) hold for a sample with the metal gate; only changing $\ln(1/k_x \ell_T)$ by $\ln(d/\ell_T)$, if $\ln(d/\ell_T)$ is large. Notice that here $Im\bar{\omega}(k_x) \equiv Im\omega(k_x)$, since only real k_x is used in the present study. Furthermore, due to assumed $k_x \ell_T \ll 1$ and $\xi \ll 1$ typically we have $S \approx ReS$.

A. Helical edge magnetoplasmon for very strong dissipation regime

Here we are now looking for weakly damped EMPs, $Re\bar{\omega}(k_x)/[-Im\omega(k_x)] \gg 1$. From a detailed analysis of the pure modes (monopole, quadrupole, dipole and octupole) spectra and their change when only the coupling with one neighboring pure mode is considered, we conclude that merely the renormalized monopole mode can be the candidate. Indeed, both for the strong and the weak dissipation regimes, it was found³⁴ that when only the $n = 0$ term is considered in Eq. (6) together with the $m = 0$ equation for $\rho_0^s(\omega, k_x)$ in Eq.(8) ($-Im\bar{\omega}(k_x)/|S'| \approx 0.12$ is almost six times larger than the same ratio for the partly renormalized monopole EMP in the limit of $k_x \ell_T \rightarrow 0$ when two terms ($n = 0, 1$) in Eq. (6) are taken into account. In the latter case two equations from Eq. (8), with $m = 0, 1$, for $\rho_{0,1}^s(\omega, k_x)$ are considered. This shows that for the monopole EMP, even for the weak or the strong dissipation, both the one term and the two terms approximations do not show good convergence in calculation of $Im\bar{\omega}$, while for $Re\bar{\omega}$ both these approximations already demonstrate a very good convergence. Moreover, for very strong dissipation, our present treatment of the general dispersion relation obtained within two terms approximation (for two coupled symmetric EMPs) as³⁴

$$\begin{aligned}
\omega_\pm^s &= k_x v_g + \frac{1}{2} [S(r_{00}^s + r_{11}^s) + S'(g_{00}^s + g_{11}^s)] \\
&\pm \frac{1}{2} \{ [S(r_{00}^s - r_{11}^s) + S'(g_{00}^s - g_{11}^s)]^2 \\
&+ 4(Sr_{01}^s + S'g_{01}^s)(Sr_{10}^s + S'g_{10}^s) \}^{1/2}, \tag{12}
\end{aligned}$$

shows that $-Im\bar{\omega}(k_x)/|S'|$ can be even less than 0.02 for $k_x \ll 1/\ell_T$. In addition, it changes sign (e.g., at $1/k_x\ell_T \approx 150$ for $\xi = 0.1$) and then its modulus quickly tends to a small value, $\approx 1.5 \times 10^{-2}$, as k_x further decreases. It is clear that obviously unphysical positive values of $Im\omega$ are due to lack of precision of the two-term expansion for the ‘‘monopole’’ EMP at very strong dissipation regime.

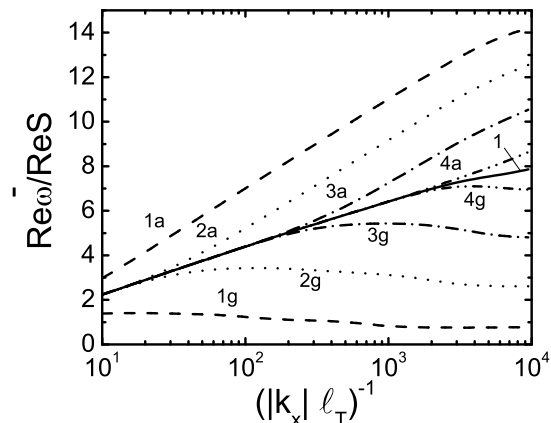


FIG. 1. Dimensionless shifted phase velocity of the helical edge magnetoplasmon, $Re\bar{\omega}/ReS = (\pi\hbar\epsilon/e^2)[Re\omega/k_x - v_g]$, as a function of $1/k_x\ell_T$ for $\nu = 1$, $\xi = 0.1$ in the regime of very strong dissipation. The solid curve (1) corresponds to a homogeneous sample. The lower (upper) dashed /1g(1a)/, dotted /2g(2a)/, dot-dashed /3g(3a)/, and dot-dot-dashed /4g(4a)/ curves correspond to a sample with the gate (air half-space) at $d = 10^{-5}$, 10^{-4} , 10^{-3} and 10^{-2} cm, respectively.

Point out that, in principle, above analytical considerations give a chance for existence, even at $\eta_T \gg 1$, of a *window of transparency* for a ‘‘renormalized monopole’’ EMP; i.e., a finite range of k_x in which the condition of weak damping can be satisfied. Now we will show the possibility of a window of transparency at very strong dissipation regime. The results presented in all figures are calculated by keeping seven terms, $n = 0, \dots, 6$, in the Eq.(6) and using seven equations, $m = 0, \dots, 6$, from Eq.(8), that leads to a 7×7 linear system of homogeneous equations. The condition of a nontrivial solution gives the dispersion relations for seven renormalized EMP modes: monopole, dipole, quadrupole, etc. The seventh term approximation shows very good convergence for the properties of the renormalized monopole, dipole, and quadrupole EMP modes. However, the only EMP mode that we will show in Figs. 1-3 is the renormalized monopole EMP.

In Fig. 1 we plot the shifted dimensionless phase velocity, $Re\bar{\omega}/ReS$, of the renormalized monopole EMP as a function of k_x for $\nu = 1$ and $\xi = 0.1$. Here, for the model confining potential Eq. (1), it is used $B = 4.1$ T, $T = 9$ K, $\omega_c/\Omega = 30$, $E_{F0} = \hbar\omega_c$; then $\ell_T \approx 4.2 \times 10^{-6}$

cm, $2\ell_T/\ell_0 \approx 6.6$, the 2DES density $n_0 \approx 10^{11}cm^{-2}$ and $v_g > s$. Point out, self-consistent many-body results of Ref.⁴⁰ for v_g give $\xi = 0.1$ and $v_g \approx 4.6 \times 10^5$ cm/sec $> s$, e.g., for $B \approx 15.7$ T, $T \approx 10$ K; $2\ell_T/\ell_0 \approx 4.0$, $n_0 \approx 3.8 \times 10^{11}cm^{-2}$.

From Fig. 1 it is seen that the shifted phase velocity decreases (increases) when the sample with metal gate (air half-space) is considered as compared with that in the homogeneous sample. Notice that this phase velocity is induced by electron-electron interactions and it is as well dependent on the dissipative wave processes.

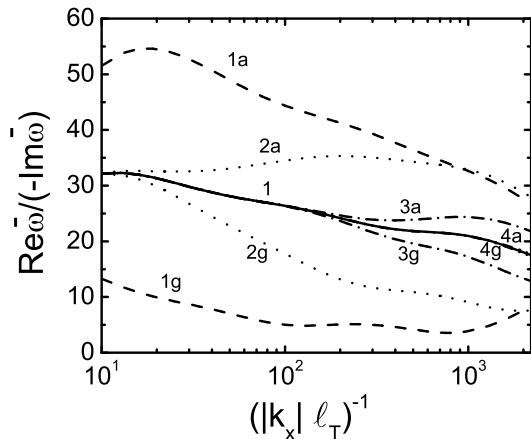


FIG. 2. Plot of $Re\bar{\omega}/(-Im\bar{\omega}) = Re(\omega - k_x v_g)/(-Im\omega)$ as a function of $1/k_x\ell_T$ for the helical edge magnetoplasmon in the very strong dissipation regime. The parameters are the same as in Fig. 1. The solid and lower (upper) dashed, dotted, dot-dashed, dot-dot-dashed curves correspond to pertinent curves in Fig. 1. For the homogeneous sample (the solid curve) there is a clear window of transparency, where $Re\bar{\omega}/(-Im\bar{\omega}) \gg 1$, due to electron-electron interactions. It is seen that when the gate is very close to the 2DES, the window of transparency is essentially suppressed since the electron-electron interaction become very weak due to screening effects.

In Fig. 2, we plot $Re\bar{\omega}/(-Im\bar{\omega})$ of the renormalized monopole mode in the actual region of k_x , for the same samples as in Fig. 1. We observe a very clear window of transparency in the wide range $2 \times 10^3 \gtrsim (k_x\ell_T)^{-1} \gtrsim 10^2$ to this mode, in which the very strong dissipation regime is achieved. In this k_x -range the renormalized monopole EMP (helical edge magnetoplasmon) is weakly damped, despite of very strong dissipation. Our analysis shows that all other EMPs (both symmetric and antisymmetric) are quite strongly damped with $-Im\bar{\omega}/Re\bar{\omega} \gtrsim \eta_T \gg 1$. From Fig. 2 we see that: (i) the gate screening decreases $Re\bar{\omega}/(-Im\bar{\omega})$, but the helical edge magnetoplasmon mode is still weakly damped for $d \gg \ell_T$; (ii) the effect of the air half-space in the sample increases $Re\omega/(-Im\omega)$ as compared with the homogeneous sample.

In order to evaluate the spatial structure of the helical edge magnetoplasmon, we solve, for a given k_x

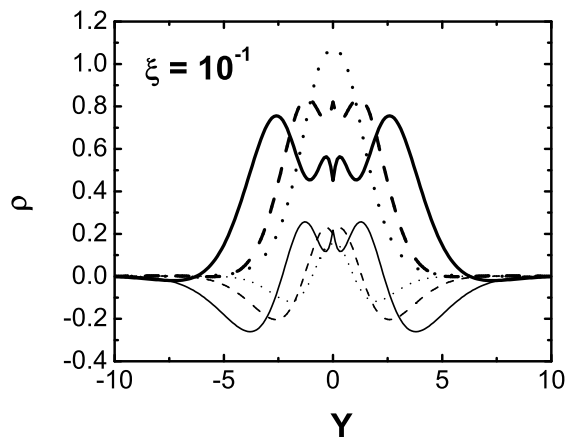


FIG. 3. Dimensionless charge density profile $\rho(Y)$ of helical edge magnetoplasmon for conditions of Figs. 1, 2 for the homogeneous sample; $\nu = 1$, $\xi = 0.1$. The solid, dashed and dotted curves correspond to $\eta_T = 10^2$, 10 and 1, respectively. The thick and the thin curves correspond to the wave phase $\phi = (Re\omega t - k_x x)$ equal to $2\pi N_k$ and $\pi/2 + 2\pi N_n$, respectively, with any integer N_k, N_n ; in particular, for $N_k = N_n$.

and correspondent complex dispersion $\bar{\omega} = \bar{\omega}(k_x)$, the linear system of $(N - 1) \times (N - 1)$ independent inhomogeneous equations for the $(N - 1)$ variables defined by $\rho_j(\bar{\omega}(k_x), k_x)/\rho_0(\bar{\omega}(k_x), k_x)$, $j = 1, \dots, N - 1$. Using these values in Eq.(6) we calculate the normalized charge density profile $\tilde{\rho}^s(\bar{\omega}, k_x, Y) = 4\ell_T \rho^s(\bar{\omega}, k_x, Y)/\rho_0^s(\bar{\omega}, k_x)$. Since this function is complex, we plot in Fig. 3 the density profile $\rho(Y) \equiv \rho^s(Y, k_x) = Re[\tilde{\rho}^s(\bar{\omega}, k_x, |Y|) \times \exp(i\phi)]$ for two sets of the wave phase ϕ . Thick and thin curves correspond to $\phi = 2\pi N_k$ and $\pi/2 + 2\pi N_n$, where N_k, N_n can be any integer. In Fig. 3 the density profiles are calculated from the 6×6 systems of linear inhomogeneous equations: for the solid curves $Re\bar{\omega}/ReS = 0.06372$ and $Im\bar{\omega}/ReS = -0.00327$, for the dashed curves $Re\bar{\omega}/ReS = 0.44132$ and $Im\bar{\omega}/ReS = -0.01712$, and for the dotted curves (plotted for comparison as the condition of very strong dissipation is not satisfied for them, while it holds for the solid and the dashed curves) $Re\bar{\omega}/ReS = 2.236$ and $Im\bar{\omega}/ReS = -0.0621$. It can be seen that for $\phi = 2\pi N_{k,n}$ the density profiles have large monopole contributions that lead to $\int_{-\infty}^{\infty} dY \rho(Y) \neq 0$. On the other hand, for $\phi = \pi/2 + 2\pi N_{k,n}$ the monopole contribution to $\rho(Y)$ is nullified so $\int_{-\infty}^{\infty} dY \rho(Y) = 0$. Fig. 3 clearly shows a strong presence of the multipole contributions, in particular, the quadrupole one.

Even though in Figs. 1-3 we have used $\xi = 0.1$, similar qualitative results are obtained for $10^{-1} \gtrsim \xi \gtrsim 10^{-3}$ which corresponds to realistic values $v_g > s$.

B. Fundamental mode in the weak dissipation regime

The treatment of the damping rate for the fundamental (or monopole) EMP in the weak dissipation regime, $\eta_T \ll 1$, was given in Ref. 34. However, the result was obtained by keeping only two terms in the expansion of Eq.(6). As it was pointed out above this approximation is rather rough for determination of the damping rate. Now we will show, in particular, that three terms expansion, in Eq.(6), well approximates the exact result for $Im\omega$ of the fundamental EMP of $n = 0$ LL.

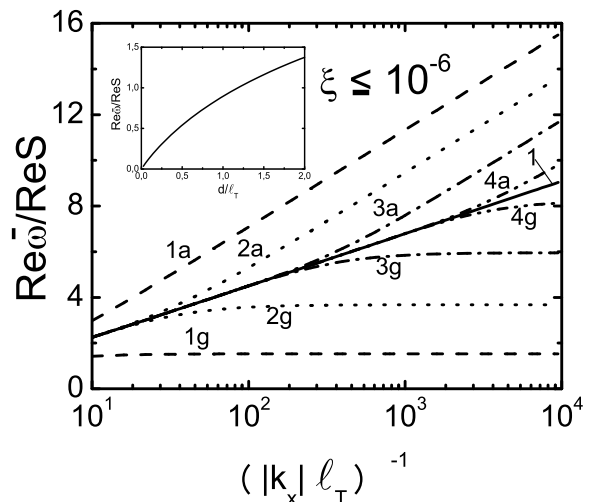


FIG. 4. Dimensionless shifted phase velocity, $Re\bar{\omega}/ReS$, of the fundamental EMP of the $N = 0$ LL, for $\xi \leq 10^{-6}$, within the long-wavelength region where $10^{-1} \geq \eta_T \geq 10^{-4}$ or smaller. As in Fig. 1, the solid curve (1) corresponds to a homogeneous sample; the lower (upper) dashed /1g(1a)/, dotted /2g(2a)/, dot-dashed /3g(3a)/, and dot-dot-dashed /4g(4a)/ curves correspond to a sample with the gate (air half-space) at $d = 10^{-5}, 10^{-4}, 10^{-3}$ and 10^{-2} cm, respectively. The inset shows $Re\bar{\omega}/ReS$ as a function of d/ℓ_T for a k_x range where the dispersion is purely acoustic in the case of the sample with a gate. Only for $d/\ell_T \lesssim 10^{-1}$ this dependence becomes linear and it is well approximated by $Re\bar{\omega}/k_x \approx (\pi\sigma_{yx}^0/\epsilon)(d/\ell_T)$.

In Fig. 4 we depict the dimensionless shifted phase velocity, $Re\bar{\omega}/ReS$, of the fundamental EMP for $\xi \leq 10^{-6}$, $\nu = 1$ and $\ell_T \approx 4.2 \times 10^{-6}$ cm, in the long-wavelength interval given by $10^4 \geq (k_x \ell_T)^{-1} \geq 10$, where $10^{-1} \geq \eta_T \geq 10^{-4}$ (or smaller, if $\eta_T < 10^{-6}$) in such a way that the condition of weak dissipation is well satisfied. For a given d it is seen that the curves for a sample with gate or air are almost equal to the solid curve if $(k_x \ell_T)^{-1} \leq d/2\ell_T$. However, for $(k_x \ell_T)^{-1} > d/2\ell_T$ the curves for a sample with gate or air begin to depart from the solid curve. In particular, for the sample with gate, the dispersion tends to be acoustic-like, $Re\omega/k_x = \text{const}$. The inset in the Fig. 4 shows $Re\bar{\omega}/ReS$ as a function of d/ℓ_T for a k_x range where the mode dispersion is purely acoustic in the sample with a gate. We point out that

the distance dependence of $Re\bar{\omega}/ReS$ is linear only for $d/\ell_T \leq 10^{-1}$. Using only one term in the expansion of Eq.(6), we obtain $Re\bar{\omega}/k_x \approx 2\pi[2ln(2) - 1](\sigma_{yx}^0/\epsilon)(d/\ell_T)$ for $d/\ell_T \ll 1$. When more terms are taken into account the shifted phase velocity increases slightly and it is better approximated by $Re\bar{\omega}/k_x \approx (\pi\sigma_{yx}^0/\epsilon)(d/\ell_T)$. These asymptotic values are in qualitative agreement with estimates given in Ref.³⁸ for the phase velocity of the EMP in a sample with the gate very close to the 2DES. Note that in GaAs based samples $\xi \ll 10^{-3}$ can be achieved only for $v_g < s$. Here, for the model confining potential Eq. (1), it is used: $B = 4.1T$, $T = 4.5K$, $\omega_c/\Omega = 60$, $E_{F0} = \hbar\omega_c$ and we have $v_g < s$.

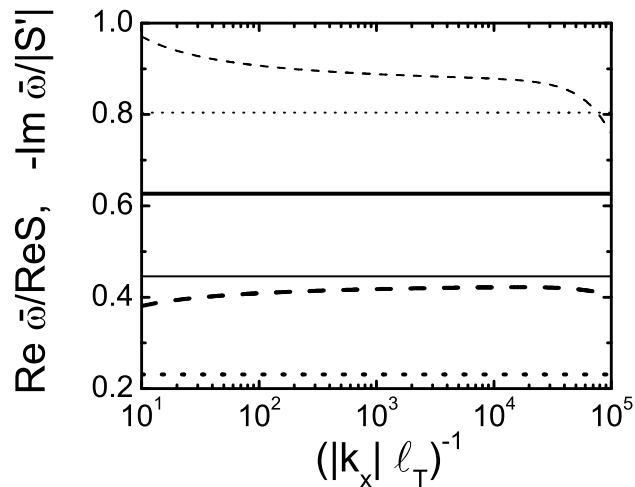


FIG. 5. Dimensionless shifted phase velocity $Re\bar{\omega}/ReS$ (thick curves) and dimensionless imaginary part of frequency (thin curves) for dipole, quadrupole and octupole $\nu = 1$ EMPs plotted for a weak dissipation ($\xi = 10^{-6}$) by the solid, the dashed, and the dotted curves, respectively. These curves are almost the same for other values of ξ within the weak dissipation regime.

In Fig. 5 at $\nu = 1$ for $\xi = 10^{-6}$, i.e., within the weak dissipation regime, $\eta_T \ll 1$, we present by the thin curves the dimensionless damping rate, $-Im\bar{\omega}/|S'|$, and by the thick curves the dimensionless shifted phase velocity, $Re\bar{\omega}/ReS$. The solid, the dashed, and the dotted curves correspond to the dipole, the quadrupole, and the octupole EMPs. These results are obtained from the solution of the 7×7 system of linear homogeneous equations for symmetric and antisymmetric EMPs, when a very good convergence is achieved for the dispersion relations. From Fig. 5 it is seen that only the shifted phase velocity and the damping rate of the quadrupole EMP (the second symmetric mode) are dependent on k_x . Those for the dipole and octupole EMPs (first two antisymmetric modes) are independent of k_x . We see that the ratio $Re\bar{\omega}/Im\bar{\omega}$ for the dipole EMP is larger than that for the quadrupole EMP. The latter is larger than that for the octupole EMP. The same holds for the shifted

phase velocity. As expected, the dipole EMP is the most weakly damped after the fundamental EMP of $n = 0$ LL in the weak dissipation regime at $\nu = 1$. Although Fig. 5 is pertinent to the homogeneous sample, the effect of the gate or air half-space on these higher-order EMP modes is negligible for any k_x if $d/\ell_T \gg 1$.

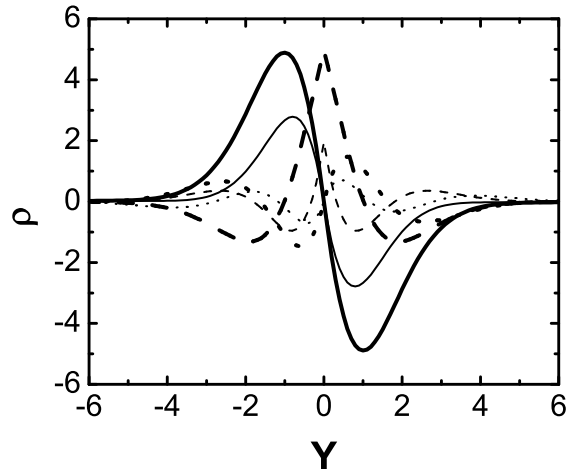


FIG. 6. Dimensionless charge density profile $\rho(Y)$ for conditions taken from Fig. 5; in particular, $\xi = 10^{-6}$, $\eta_T = 10^{-2}$, and $k_x \ell_T = 10^{-4}$. The thick and thin curves correspond to the wave phase $\phi = 2\pi N_k$ and $\pi/2 + 2\pi N_n$, respectively, for any integer N_k, N_n ; the thin curves plot $10 \times \rho(Y)$. The solid, dashed and dotted curves correspond to the dipole, the quadrupole, and the octupole EMPs, respectively.

In Fig. 6, we show the charge density profile $\rho(Y) \equiv \rho_{s,a}(Y, k_x) = Re[\check{\rho}_{s,a}(\bar{\omega}, k_x, Y) \times \exp(i\phi)]$ of the higher-order EMPs for two sets of the wave phase ϕ and $\xi = 10^{-6}$. The charge density for dipole, quadrupole and octupole EMPs is indicated by thick (thin) solid, dashed and dotted curves, respectively, for $\eta_T = 10^{-2}$. The curves were calculated from the 6×6 system of linear inhomogeneous equations. The thick and thin curves correspond to $\phi = 2\pi N_k$ and $\pi/2 + 2\pi N_n$, respectively. The thin curves are $10 \times \rho$. In Fig. 6, we have $\bar{\omega} = 0.626S + 0.446S'$ for the solid curves, $\bar{\omega} = 0.422S + 0.878S'$ for the dashed curves and $\bar{\omega} = 0.231S + 0.804S'$ for the dotted curves. We observe that the density profiles of the dipole EMP is not modified qualitatively by varying the wave phase ϕ .

IV. FUNDAMENTAL EMPs AT $\nu = 4$

Now, assuming the weak dissipation at the $\nu = 4$ QHE regime, we will treat fundamental EMPs omitting dissipation. For definiteness, only the model confining potential Eq. (1) is considered. Then, instead of Eq. (5), the integral equation is given as

$$\begin{aligned}
& \sum_{n=0}^1 (\omega - k_x v_{gn}) \rho_n(\omega, k_x, y) - \tilde{S} \sum_{n=0}^1 R_{0n}(y) \\
& \times \int_{-\infty}^{\infty} dy' [\beta K_0(|k_x| \sqrt{(y-y')^2 + 4d^2}) \\
& + K_0(|k_x||y-y'|)] \sum_{m=0}^1 \rho_m(\omega, k_x, y') = 0, \quad (13)
\end{aligned}$$

where $\tilde{S} = (2\tilde{\sigma}_{yx}^0/\epsilon)k_x$, $\tilde{\sigma}_{yx}^0 = e^2/\pi\hbar$, $R_{0n}(y) = R_{0n}(\bar{y}_n) = (4\ell_{Tn})^{-1} \cosh^{-2}(\bar{y}_n/2\ell_{Tn})$, $\ell_{Tn} = \ell_0 k_B T / \hbar v_{gn}$, and $v_g = \hbar\Omega^2 k_{re}^{(n)} / m^* \omega_c^2$ is the group velocity of the edge states of the n -th LL; $\bar{y}_n = y - y_{re}^{(n)}$, $y_{re}^{(n)} = \ell_0^2 k_{re}^{(n)}$, $n = 0, 1$. The Hall conductivity in the inner part of the channel is given by $\sigma_{yx}^0 = 2\tilde{\sigma}_{yx}^0 = 2e^2/\pi\hbar$. We assume that $2\ell_{Tn}/\ell_0 \gg 1$ and the long-wavelength limit $|k_x|\ell_{Tn} \ll 1$, $|k_x|\Delta y_{01} \ll 1$, where $\Delta y_{01} = y_{re}^{(0)} - y_{re}^{(1)}$. In addition, it was assumed in Eq.(13) that $\Delta y_{01}/\ell_{T1} \gg 1$ and the charge density distortion of the n -th LL is localized nearby its edge, $y_{re}^{(n)}$. Note that the LLs spectra for our model Eq. (1) give that $v_{g1} < v_{g0}$ and, hence, $\ell_{T1} > \ell_{T0}$. We can look for the solution of Eq.(13) as

$$\rho(\omega, k_x, y) = \sum_{n=0}^1 \rho_n(\omega, k_x, y), \quad (14)$$

where $\rho_n(\omega, k_x, y)$ are localized within a region of length of the order of ℓ_{Tn} around the edge of the n -th LL. To study fundamental EMPs of the $n = 0, 1$ LLs, $\rho_n(\omega, k_x, y) \equiv \rho_n(\omega, k_x, \bar{y}_n)$ is well approximated by

$$\rho_n(\omega, k_x, \bar{y}_n) = R_{0n}(\bar{y}_n) \rho_n(\omega, k_x). \quad (15)$$

Indeed, for $k_x \rightarrow 0$ the solution of Eq. (13) given by Eqs. (14), (15) is almost exact. Furthermore, as we have shown in previous sections, similar approximations for the fundamental EMP of $n = 0$ LL at $\nu = 1$ (2) yield very accurate results for the dispersion relation and the charge density profile for all k_x . However, now the symmetry of the problem with respect to $y_{re}^{(0)}$ or $y_{re}^{(1)}$ is broken due to the presence of the inter-edge Coulomb interaction.

Neglecting by small overlapping between $\rho_0(\omega, k_x, \bar{y}_0)$ and $\rho_1(\omega, k_x, \bar{y}_1)$, we multiply Eq.(13) by $\tilde{R}_{0n}^{-1}(Y_n)$, where $\tilde{R}_{0n}(Y_n) = \exp(|Y_n|) R_{0n}(Y_n)$, and integrate over $Y_n = \bar{y}_n/\ell_{Tn}$ from $-\infty$ to ∞ . Then, taking into account Eqs. (14) and (15), the coupled system of two equations for $\rho_n \equiv \rho_n(\omega, k_x)$ is given by

$$\begin{aligned}
& [\omega - (k_x v_{g0} + \tilde{S}A_{00}/2)]\rho_0 - (\tilde{S}A_{01}/2)\rho_1 = 0, \\
& -(\tilde{S}A_{01}/2)\rho_0 + [\omega - (k_x v_{g1} + \tilde{S}A_{11}/2)]\rho_1 = 0, \quad (16)
\end{aligned}$$

where

$$\begin{aligned}
A_{mn}(k_x) &= \frac{1}{4} \int_{-\infty}^{\infty} dx \int_{-\infty}^{\infty} dx' \exp(-|x|) \cosh^{-2}(x'/2) \\
& \times [\beta K_0(|k_x|\ell_{Tn} \sqrt{(\tilde{x}_{mn}(x) - x')^2 + (2d/\ell_{Tn})^2}) \\
& + K_0(|k_x|\ell_{Tn} |\tilde{x}_{mn}(x) - x'|)], \quad (17)
\end{aligned}$$

with $\tilde{x}_{mn}(x) = (\Delta y_{mn}/\ell_{Tn}) + (\ell_{Tm}/\ell_{Tn})x$. Point out that as the integral term in Eq.(13) is very weakly dependent on y for the assumed very small k_x , we still can arrive to Eqs. (16), (17) even if the overlapping between $\rho_0(\omega, k_x, y)$ and $\rho_1(\omega, k_x, y)$ is not very small.

First we will study EMPs (i) for the sample without the gate ($\beta = 0$). Secondly, we will study EMPs (ii) for $d/\ell_{Tn} \gg 1$ and (iii) for $d/\ell_{Tn} \ll 1$ in the case of the sample with gate ($\beta = -1$), assuming that $|k_x|d \ll 1$. For the case (i) ($\beta = 0$) we have $A_{01} = A_{10} \approx 2[\ln(1/|k_x|\ell_{T1}) + \ln(2) - \gamma + \ln(\ell_{T1}/\Delta y_{01})]$, $A_{11} \approx 2[\ln(1/|k_x|\ell_{T1}) + \ln(2) - \gamma] - 0.25$, and $A_{00} \approx A_{11} + 2\ln(\ell_{T1}/\ell_{T0})$. Thus, despite the condition $\Delta y_{01}/\ell_{T1} \gg 1$, the system of equations, Eq.(16), is strongly coupled by the long-range Coulomb interaction between the edges of the LLs. If this inter-edge Coulomb coupling is neglected, by setting $A_{01} = 0$, the Eq.(16) yields the dispersion relations of the *decoupled* fundamental EMPs of the $n = 0$ (for $\rho_0 \neq 0$) and $n = 1$ (for $\rho_1 \neq 0$) LL's as

$$\begin{aligned}
\omega^{(n)} &= k_x v_{gn} + (2/\epsilon)\tilde{\sigma}_{yx}^0 k_x \\
& \times [\ln(1/|k_x|\ell_{Tn}) - 0.01]. \quad (18)
\end{aligned}$$

If we take into account the Coulomb coupling between these fundamental EMP's, their spectra, as it follows from Eq.(16), changes drastically. The dispersion of the renormalized fundamental EMP of the $n = 0$ LL, or the fast fundamental EMP, becomes

$$\begin{aligned}
\omega_+^{(01)} &= k_x v_{01} + (4/\epsilon)\tilde{\sigma}_{yx}^0 k_x \\
& \times [\ln(1/|k_x|\ell_c^+) + 0.05], \quad (19)
\end{aligned}$$

where $v_{01} = (v_{g0} + v_{g1})/2$, and $\ell_c^+ = \sqrt{\Delta y_{01}\ell_{T0}\ell_{T1}}$ is the characteristic length that determines the spatial dispersion of the fast mode. On turn, the renormalized fundamental EMP of the $n = 1$ LL, or the slow fundamental EMP, becomes

$$\begin{aligned}
\omega_-^{(01)} &= k_x v_{01} + (2/\epsilon)\tilde{\sigma}_{yx}^0 k_x \\
& \times \left[\ln\left(\Delta y_{01}/\sqrt{\ell_{T1}\ell_{T0}}\right) - 0.12 \right], \quad (20)
\end{aligned}$$

where the ratio of the characteristic lengths Δy_{01} and $\sqrt{\ell_{T1}\ell_{T0}}$ mainly determine the dispersion of the slow mode. It can be seen that $\omega_-^{(01)}(k_x)$ becomes purely acoustic in contrast to $\omega_+^{(01)}(k_x)$. From Eqs. (18)-(20) we conclude that renormalization of the dispersion

$\omega^{(n)}$ due to the Coulomb coupling of the charge fluctuations at the edges of $n = 0, 1$ LLs is strong as typically $\omega_+^{(01)}/\omega_-^{(01)} \gg 1$ while $\omega^{(0)}/\omega^{(1)} \approx 1$. The phase velocities of both fast and slow fundamental EMPs decrease with increasing T .

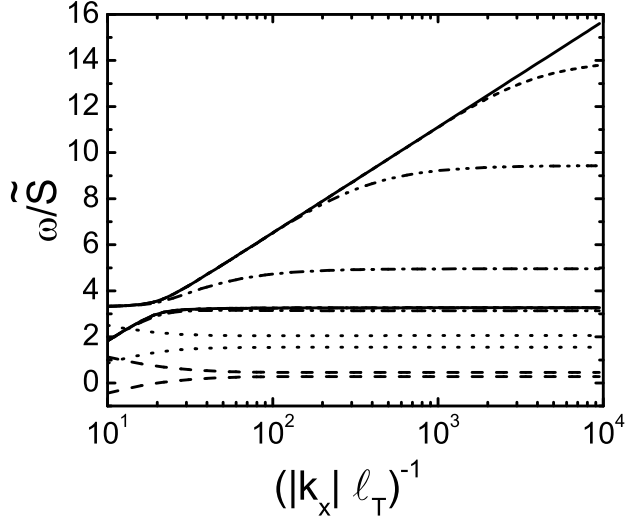


FIG. 7. Dimensionless phase velocity of the fast and the slow fundamental EMPs, for $\nu = 4$, as a function of $(k_x \ell_T)^{-1}$ calculated from Eq.(16); $\tilde{S} = (2/\epsilon)\tilde{\sigma}_{yx}^0 k_x$. The solid curves correspond to the homogeneous sample. For samples with the gate at $d = 10^{-6}$ cm ($\approx \Delta y_{01}/90$), 10^{-5} cm ($\approx \Delta y_{01}/9$), 10^{-4} cm ($\approx \Delta y_{01}$), 10^{-3} cm ($\approx 11 \times \Delta y_{01}$), and 10^{-2} cm ($\approx 110 \times \Delta y_{01}$) from the 2DES the plots are presented by the dashed, dotted, dash-dotted, dash-dot-dotted and shorted-dash curves, respectively.

For the case (ii) ($\beta = -1$ and $d/\ell_{T_n} \gg 1$) we find $A_{01} = A_{10} \approx 2 \ln(2d/\Delta y_{01})$, $A_{11} \approx 2 \ln(2d/\ell_{T1}) - 0.25$, and $A_{00} \approx 2 \ln(2d/\ell_{T0}) - 0.25$. In this case the dispersion of the fast fundamental EMP it follows from Eq. (16) as

$$\omega_+^{(01)} = k_x v_{01} + (4/\epsilon)\tilde{\sigma}_{yx}^0 k_x [\ln(2d/\ell_c^+) - 0.06], \quad (21)$$

while the slow fundamental EMP is still given by Eq.(20).

Finally, in the case (iii) ($\beta = -1$ and $d/\ell_{T_n} \ll 1$), the dispersion relation for the renormalized fundamental EMPs of $n = 0, 1$ LLs is given by

$$\omega_n^{(01)} = k_x v_{gn} + \frac{2\pi}{\epsilon} \frac{d}{\ell_{Tn}} \tilde{\sigma}_{yx}^0 k_x [2 \ln(2) - 1]. \quad (22)$$

As expected, $\omega_0^{(01)}$ is in agreement with the result for $\nu = 1, 2$, obtained in Sec. IIIB, since the fundamental EMP of $n = 0$ LL is totally decoupled from the fundamental EMP of $n = 1$ LL.

In Fig. 7 the dimensionless phase velocity, ω/\tilde{S} , for the renormalized fundamental EMPs of the $n = 0$ LL and the $n = 1$ LL is plotted as a function of $(k_x \ell_T)^{-1}$,

$\ell_T \equiv \ell_{T0}$, for $\nu = 4$ from Eq.(16). For each sample, the top curve corresponds to the fast mode and the bottom curve represents the slow mode. For the fast EMP mode only the samples with the gate can show acoustic-like dispersion, while for the slow EMP mode in all samples there is a wide region with the acoustic dispersion. Notice, for $d \lesssim 10^{-6}$ cm Eq.(21) well approximates dispersion relations for the fast fundamental EMP. Here, for a GaAs-based heterostructure, it is assumed that $B = 4.1$ T, $\omega_c/\Omega \simeq 100$, $E_{F0} = 2\hbar\omega_c$, $T = 2.66$ K; then we have $v_{g0} \approx 2.35 \times 10^5$ cm/sec $< s$, $v_{g1} \approx 1.36 \times 10^5$ cm/sec $< s$, $\ell_{T1}/\ell_{T0} = \sqrt{3}$ with $\ell_{T1} \approx 0.41 \times 10^{-5}$ cm and $2\ell_{T0}/\ell_0 \approx 3.8$. In addition, it follows that $\Delta y_{01} \approx 9.3 \times 10^{-5}$ cm and $\Delta y_{01}/\ell_{T1} \approx 22.5$.

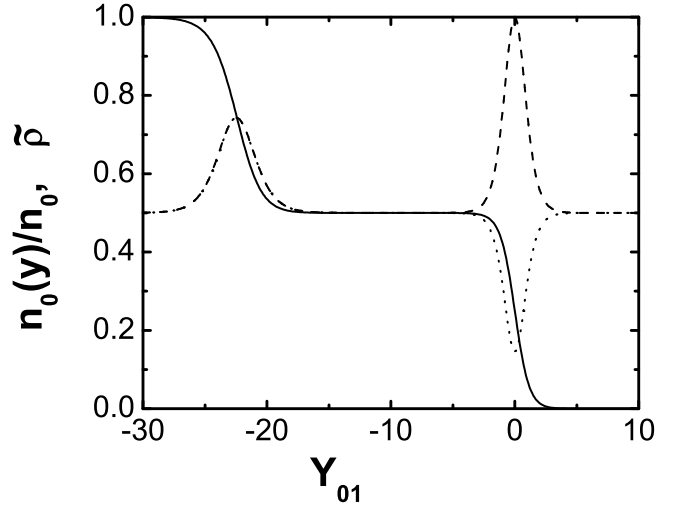


FIG. 8. The unperturbed electron density $n_0(y)$, normalized to the bulk value n_0 , and the dimensionless charge density profile $\tilde{\rho}(\omega, k_x, Y_{01}) \equiv 4\ell_{T1}\rho(\omega, k_x, Y_{01})/\rho_1$, where $Y_{01} = \bar{y}_0/\ell_{T1}$, of the renormalized fundamental EMPs for $(|k_x| \ell_{T1})^{-1} = 10^2$. The solid curve corresponds to $n_0(y)$, the dashed curve corresponds to the fast fundamental EMP, $\omega_+^{(01)}/\tilde{S} = 6.52$, and the dotted curve correspond to the slow fundamental EMP, $\omega_-^{(01)}/\tilde{S} = 3.25$. Here the same parameters are used as for the solid curves in Fig. 7. The dashed and the dotted curves plot $\tilde{\rho}/4.1$, shifted upward on 0.5.

Substituting Eqs. (19) and (20) in Eqs. (14)-(16) the charge density profiles of the fast and the slow fundamental EMPs, in the absence of gate in the sample, are given by

$$\tilde{\rho}(\omega, k_x, Y_{01}) = (\ell_{T1}/\ell_{T0}) \cosh^{-2}((\ell_{T1}/\ell_{T0}) Y_{01}/2) \tilde{\rho}_0 + \cosh^{-2}((\Delta y_{01}/2\ell_{T1}) + Y_{01}/2), \quad (23)$$

where $\tilde{\rho}(\omega, k_x, Y_{01}) = 4\ell_{T1}\rho(\omega, k_x, Y_{01})/\rho_1$, $\tilde{\rho}_0 = \rho_0/\rho_1$, and $Y_{01} = \bar{y}_0/\ell_{T1}$. In Fig. 8 for the same conditions that for the solid curves in Fig. 7 we plot the charge density profile for the fast fundamental EMP, $\frac{1}{4.1}\tilde{\rho}(\omega_+^{(01)}, k_x, Y_{01})$, by the dashed curve and for the slow fundamental EMP,

$\frac{1}{4\pi}\tilde{\rho}(\omega_{-}^{(01)}, k_x, Y_{01})$, by the dotted curve. In Fig. 8 it is assumed that $y_{re}^{(0)} = 0$; $y_{re}^{(1)}/\ell_{T1} = -\Delta y_{01}/\ell_{T1} \approx -22.5$ and $y_r/\ell_{T1} \approx -53.2$.

V. CONCLUDING REMARKS

In present microscopic treatment of EMPs we, e.g., similar to Refs.^{24,26}, have neglected the diffusion current. Here this approximation is well justified, except for the charge density profiles $\rho(Y)$ of the symmetric modes within a very narrow region, $|Y| \ll \ell_T$, as it is seen in Figs. 3, 6. Where small finite cusps (notice, in Ref.²⁴ the cusp of density is infinite, without the diffusion current) are present. Indeed, in the absence of the diffusion current, for symmetric modes our equations warrant at $Y = 0$ the continuity of $\rho(Y)$, however, not of its first derivative, $d\rho(Y)/dY$; inclusion of the diffusion current will make $d\rho(Y)/dY$ continuous at $Y = 0$ as well. So, cf. with Ref.²⁴, when the diffusion current is taken into account it will only smooth out these small cusps, without any essential effect as on the EMPs spectra so on the charge density profile.

In present study, it is used simple analytical model, Eq. (1), for the confining potential $V'(y)$ (in addition, for some figures we present also the estimations that include the effect of many-body interactions⁴⁰). This analytical model reproduces quite well the confining potential of a wide channel calculated numerically in the Hartree approximation^{34,43,44}. Moreover, present treatment can be easily extended for the confining potentials of different forms if they are smooth on the scale of ℓ_0 and the not-too-low temperatures conditions are satisfied. In particular, the group velocity of the edge states v_g renormalized by self-consistent exchange-correlation effects can be finite even if the Hartree approximation group velocity $v_g^H = 0$ ⁴⁰. The latter condition corresponds to the LL flattening and the formation of the compressible strip⁴⁵, cf. with^{46,47} and⁴⁴. Notice that with exchange and correlation interactions included within density functional theory approximation (rather crude for 2DES in the quantum Hall regime, see, e.g.,⁴³) also it is found that for realistic parameters the exchange interaction can completely suppress the formation of compressible strips⁴⁴.

So the applicability of our present results may have substantially wider temperatures range than $30\text{K} \gtrsim T \gtrsim 10\text{K}$. Furthermore, we can speculate that treated here model and helical edge magnetoplasmon at not-too-low temperatures can be relevant to EMPs interference observed recently¹⁶⁻¹⁸ for temperatures $\leq 80\text{K}$ as it, in particular, needs weakly damped EMPs.³⁷

ACKNOWLEDGMENTS

We thank Nelson Studart for many useful discussions. This work was supported by Brazilian FAPEAM

(Fundação de Amparo à Pesquisa do Estado do Amazonas) Grants; this work of O. G. B. was also supported by Brazilian CNPq Grant.

- ¹S. J. Allen, H. L. Stormer, and J. C. M. Hwang, Phys. Rev. B **28**, 4875 (1983).
- ²D. B. Mast, A. J. Dahm, and A. L. Fetter, Phys. Rev. Lett. **54**, 1706 (1985).
- ³D. C. Glattli, E. Y. Andrei, G. Deville, J. Poitrenaud, and F. I. B. Williams, Phys. Rev. Lett. **54**, 1710 (1985).
- ⁴S. A. Govorkov, M. I. Reznikov, A. P. Senichkin, and V. I. Talyanskii, Pis'ma Zh. Eksp. Teor. Fiz. **44**, 380 (1986) [JETP Lett. **44**, 487 (1986)]; V. A. Volkov, D. V. Galchenkov, L. A. Galchenkov, I. M. Grodnenskii, O. R. Matov, and S. A. Mikhailov, Pis'ma Zh. Eksp. Teor. Fiz. **44**, 510 (1986) [JETP Lett. **44**, 655 (1986)].
- ⁵V. I. Talyanskii, I. E. Batov, B. K. Medvedev, J. P. Kotthaus, M. Wassermeier, A. Wixforth, J. Weimann, W. Schlapp, and H. Nickel, Pis'ma Zh. Eksp. Teor. Fiz. **50**, 196 (1989) [JETP Lett. **50**, 221 (1989)].
- ⁶M. Wassermeier, J. Oshinowo, J. P. Kotthaus, A. H. MacDonald, C. T. Foxon, and J. J. Harris, Phys. Rev. B **41**, 10287 (1990).
- ⁷I. Grodnensky, D. Heitmann, and K. von Klitzing, Phys. Rev. Lett. **67**, 1019 (1991); Surface Science **263**, 467 (1992).
- ⁸R. C. Ashoori, H. L. Stormer, L. N. Pfeiffer, K. W. Baldwin, and K. West, Phys. Rev. B **45**, 3894 (1992).
- ⁹V. I. Talyanskii, A. V. Polisski, D. D. Arnone, M. Pepper, C. G. Smith, D. A. Ritchie, J. E. Frost, and G. A. C. Jones, Phys. Rev. B **46**, 12427 (1992).
- ¹⁰N. B. Zhitenev, R. J. Haug, K. v. Klitzing, and K. Eberl, Phys. Rev. Lett. **71**, 2292 (1993); Phys. Rev. B **49**, 7809 (1994).
- ¹¹V. I. Talyanskii, D. R. Mace, M. Y. Simmons, M. Pepper, A. C. Churchill, J. E. F. Frost, D. A. Ritchie and G. A. C. Jones, J. Phys. Condens. Matter **7**, L435 (1995).
- ¹²G. Ernst, R. J. Haug, J. Kuhl, K. von Klitzing, and K. Eberl, Phys. Rev. Lett. **77**, 4245 (1996).
- ¹³E. V. Deviatov, V. T. Dolgoplov, F. I. B. Williams, B. Jager, A. Lorke, J. P. Kotthaus, A. C. Gossard, Appl. Phys. Lett. **71**, 3655 (1997).
- ¹⁴N. Q. Balaban, U. Meirav, H. Shtrikman, and V. Umansky, Phys. Rev. B **55**, R13397 (1997); N. Q. Balaban, U. Meirav, and I. Bar-Joseph, Phys. Rev. Lett. **81**, 4967 (1998).
- ¹⁵G. Sukhodub, F. Hohls, and R. J. Haug, Phys. Rev. Lett. **93**, 196801 (2004).
- ¹⁶I. V. Kukushkin, M. Yu. Akimov, J. H. Smet, S. A. Mikhailov, K. von Klitzing, I. L. Aleiner, and V. I. Falko, Phys. Rev. Lett. **92**, 236803 (2004).
- ¹⁷I. V. Kukushkin, S. A. Mikhailov, J. H. Smet, and K. v. Klitzing, Appl. Phys. Lett. **86**, 044101 (2005).
- ¹⁸P. S. Dorozhkin, S. V. Tovstonog, S. A. Mikhailov, I. V. Kukushkin, J. H. Smet, and K. v. Klitzing, Appl. Phys. Lett. **87**, 092107 (2005).
- ¹⁹O. I. Kirichek, P. K. H. Sommerfeld, Yu. P. Monarkha, P. J. M. Peters, Yu. Z. Kovdrya, P. P. Steijaert, R. W. van der Heijden, and A. T. A. M. de Waele, Phys. Rev. Lett. **74**, 1190 (1995).
- ²⁰X. G. Wen, Phys. Rev. B **43**, 11025 (1991).
- ²¹A. Melikidze and Kun Yang, Phys. Rev. B **70**, 161312(R) (2004).
- ²²Wei-Cheng Lee, N. A. Sinitsyn, Emiliano Papa, and A. H. MacDonald, Phys. Rev. B **72**, 121304(R) (2005).
- ²³A. L. Fetter, Phys. Rev. B **33**, 3717 (1986).
- ²⁴V. A. Volkov and S. A. Mikhailov, Zh. Eksp. Teor. Fiz. **94**, 217 (1988) [Sov. Phys. JETP **67**, 1639 (1988)]; in *Modern Problems in Condensed Matter Sciences*, edited by V. M. Agranovich and A. A. Maradudin (North-Holland, Amsterdam, 1991), Vol. 27.2, Ch. 15, p. 885.
- ²⁵M. Stone, Ann. Phys. (NY) **207**, 38 (1991); M. Stone, H. W. Wyld, and R. L. Schult, Phys. Rev. B **45**, 14156 (1992).
- ²⁶I. L. Aleiner and L. I. Glazman, Phys. Rev. Lett. **72**, 2935 (1994).
- ²⁷C. de Chamon and X. G. Wen, Phys. Rev. B **49**, 8227 (1994).
- ²⁸S. Giovanazzi, L. Pitaevskii, and S. Stringari, Phys. Rev. Lett. **72**, 3230 (1994).

- ²⁹J. H. Han and D. J. Thouless, Phys. Rev. B **55**, R1926 (1997).
- ³⁰U. Zulicke, R. Bluhm, V. A. Kostecky, and A. H. MacDonald, Phys. Rev. B **55**, 9800 (1997).
- ³¹O. G. Balev and P. Vasilopoulos, Phys. Rev. B **56**, 13252 (1997).
- ³²O. G. Balev and P. Vasilopoulos, Phys. Rev. Lett. **81**, 1481 (1998); O. G. Balev, P. Vasilopoulos, and Nelson Studart, J. Phys.: Condens. Matt. **11**, 5143 (1999).
- ³³O. G. Balev and P. Vasilopoulos, Phys. Rev. B **59**, 2807 (1999).
- ³⁴O. G. Balev and Nelson Studart, Phys. Rev. B **61**, 2703 (2000).
- ³⁵T. H. Hansson and S. Viefers, Phys. Rev. B **61**, 7553 (2000).
- ³⁶M. D. Johnson and G. Vignale, Phys. Rev. B **67**, 205332 (2003).
- ³⁷S. A. Mikhailov, Appl. Phys. Lett. **89**, 042109 (2006).
- ³⁸N. B. Zhitenev, R. J. Haug, K. v. Klitzing, and K. Eberl, Phys. Rev. B **52**, 11277 (1995).
- ³⁹O. G. Balev and P. Vasilopoulos, Phys. Rev. B **47**, 16410 (1993); O. G. Balev, P. Vasilopoulos, and E. V. Mozdor, Phys. Rev. B **50**, 8706 (1994); O. G. Balev and P. Vasilopoulos, Phys. Rev. B **50**, 8727 (1994).
- ⁴⁰I. O. Baleva, Nelson Studart, and O. G. Balev, Phys. Rev. B **65**, 073305 (2002).
- ⁴¹Here $A(\omega, k_x, y)$ is the wave amplitude of any wave physical value involved in an EMP, e.g.: of the electron charge density, of the electric potential, any component of the electric field or of the current density.
- ⁴²E.g., for pure monopole mode most close neighboring pure mode there is quadrupole one as coupling it is possible only among pure modes of the same parity.³⁴
- ⁴³O. G. Balev and Nelson Studart, Phys. Rev. B **64**, 115309 (2001).
- ⁴⁴S. Ihnatsenka and I. V. Zozoulenko, Phys. Rev. B **73**, 075331 (2006); Phys. Rev. B **73**, 155314 (2006); Phys. Rev. B **78**, 035340 (2008).
- ⁴⁵D. B. Chklovskii, B. I. Shklovskii, and L. I. Glazman, Phys. Rev. B **46**, 4026 (1992).
- ⁴⁶L. Brey, J. J. Palacios, and C. Tejedor, Phys. Rev. B **47**, 13884 (1993).
- ⁴⁷T. Suzuki and Tsuneya Ando, J. Phys. Soc. Jpn. **62**, 2986 (1993); Physica B **201**, 345 (1994).